ORIGINAL ARTICLE

Pattern Formation in a Model for Mountain Pine Beetle Dispersal: Linking Model Predictions to Data

S. Strohm · R.C. Tyson · J.A. Powell

Abstract Pattern formation occurs in a wide range of biological systems. This pattern formation can occur in mathematical models because of diffusion-driven instability or due to the interaction between reaction, diffusion, and chemotaxis. In this paper, we investigate the spatial pattern formation of attack clusters in a system for Mountain Pine Beetle. The pattern formation (aggregation) of the Mountain Pine Beetle in order to attack susceptible trees is crucial for their survival and reproduction. We use a reaction-diffusion equation with chemotaxis to model the interaction between Mountain Pine Beetle, Mountain Pine Beetle pheromones, and susceptible trees. Mathematical analysis is utilized to discover the spacing in-between beetle attacks on the susceptible landscape. The model predictions are verified by analysing aerial detection survey data of Mountain Pine Beetle Attack from the Sawtooth National Recreation Area. We find that the distance between Mountain Pine Beetle attack clusters predicted by our model closely corresponds to the observed attack data in the Sawtooth National Recreation Area. These results clarify the spatial mechanisms controlling the transition from incipient to epidemic populations and may lead to control measures which protect forests from Mountain Pine Beetle outbreak.

S. Strohm (✉) · R.C. Tyson
University of British Columbia Okanagan Campus, Kelowna, Canada
e-mail: shaun.strohm@gmail.com

J.A. Powell
Mathematics and Statistics, Utah State University, Logan, UT, USA

1 Introduction

Pattern formation is ubiquitous in biology (Murray 2003). Nature provides a diverse array of systems with spatial patterns. Examples include static spatial patterns such as those found on butterfly wings and mammalian coats, and spatiotemporal patterns such as those exhibited by predator-prey populations (Murray 2003). What is even more interesting is that reaction-diffusion systems can exhibit all of these various patterns given the correct range of parameter values. Pattern arises in these systems through diffusion-driven instability, which was first observed by Turing (1952). An essential element for spatial patterning is local activation with long-range inhibition (Murray 2003).

Not all of pattern formation is due to diffusion-driven instability. Pattern formation can also occur in reaction-diffusion equations with chemotaxis. Examples include models for snake pigmentation patterns and spatial patterns formed by colonies of growing bacteria (Murray 2003). In particular, Budrene and Berg (1991, 1995) found very diverse and interesting patterns formed by the bacteria *Escherichia coli* and *S. typhimurium*. Tyson et al. (1999) were able to reproduce these interesting patterns using a reaction-diffusion model which incorporated chemotaxis.

A very interesting insect to study in regard to pattern formation is the Mountain Pine Beetle (*Dendroctonus ponderosae* Hopkins, MPB). This bark beetle has had a major economic impact on the Western Canada and United States forestry industries (Safranyik and Wilson 2006). Many characteristics of the spread and spatial synchrony of MPB have been well researched at both large (Aukema et al. 2008; Gamarra and He 2008; Brooks and Stone 2003; Peltonen et al. 2002) and small (Robertson et al. 2009; Mitchell and Preisler 1991) scales. These studies have illuminated the factors driving the spatial patterns in beetle spread, such as weather, elevation and proximity to nearby MPB attacked areas. Additionally, models for MPB movement have been developed to describe the spread and aggregative behaviour of MPB (Logan et al. 1998; Bentz et al. 1996; Pérez and Dragićević 2011; Polymenopoulos and Long 1990; Safranyik and Wilson 2006; Burnell 1977; Geiszler et al. 1980; Safranyik et al. 1999; Riel et al. 2004; Heavilin and Powell 2008; Powell et al. 1998; White and Powell 1997; Hughes et al. 2006). In this paper, we will focus on the spot formation that occurs at intermediate spatial scales. Previous cluster analysis focused on either large scales (kilometres) or very small scales (100-metre regions). In this study we are interested in the pattern formation of clusters at intermediate scales, with distances between clusters falling within the 0–1000-metre range. We also focus our search to investigate spot formation in a single year rather than the change in spot formation across multiple years.

Successful aggregation of MPB (in response to a suite of pheromones) is crucial for reproduction and survival of the species. At incipient epidemic population levels, the pattern of attack of MPB on a landscape is small isolated spots (Safranyik and Wilson 2006). In contrast, there can be high mortality of host trees over thousands of contiguous acres at epidemic population levels. We are interested in understanding the pattern formed by MPB during the transition from incipient epidemic to frank outbreaks. To do this work, we investigate pattern formation via a spatially explicit model for MPB dispersal (White and Powell 1997). We then compare the model

predictions to 19 years of data from MPB attack in the Sawtooth National Recreation Area (SNRA), in Idaho, USA. We find that the distances between MPB attack clusters predicted by our model and observed in the SNRA are the same. This indicates that the biological behaviours in our model are sufficient to explain the observed attack pattern.

We first introduce our mathematical model in Sect. 2. Using pattern formation analysis in Sect. 3, we determine the wavelength in-between MPB attack clusters as predicted by our mathematical model. We then calculate the wavelength between clusters of MPB attack in the data from the SNRA and compare it to the model predictions in Sect. 4. Discussion and future work can be found in Sect. 5.

2 Mathematical Model

We are interested in the period of emergence, dispersal and attack of the MPB. These events all occur over the space of one summer: adults emerge from their host trees, then aggregate on new hosts where they mount an attack and, if successful, lay new eggs. The period between egg-laying and adult emergence occurs during the winter, and is not relevant to the modelling exercise here. That is, we are interested in understanding the attack pattern that results from the dispersal and aggregation stages of the MPB life cycle in a single summer. We thus require a model for MPB movement through forest habitat that incorporates the interaction between the beetle and its pheromones in a continuous framework over space and time. The choice of model structure is based on theoretical work by Powell et al. (1998). The model equations are

$$\frac{\partial P}{\partial t} = \overbrace{\mu_p \nabla^2 P}^{\text{diffusion}} - \overbrace{\nabla \left[\left(v_a \frac{b_0 - A}{b_0 + A/b_1} \nabla A \right) P \right]}^{\text{chemotaxis}} - \overbrace{\delta_p P}^{\text{death}} - \overbrace{\lambda P \frac{P^2}{P^2 + (k_p)^2}}^{\text{nesting}} + \overbrace{\gamma}^{\text{emergence}} ,$$

(1a)

$$\frac{\partial Q}{\partial t} = \overbrace{-\delta_q Q}^{\text{death}} + \overbrace{\lambda P \frac{P^2}{P^2 + (k_p)^2}}^{\text{nesting}},$$

(1b)

$$\frac{\partial A}{\partial t} = \overbrace{\mu_a \nabla^2 A}^{\text{diffusion}} + \overbrace{a_1 Q}^{\text{synthesis}} - \overbrace{\delta_a A}^{\text{degradation}} ,$$

(1c)

where our three variables are P—the density of flying MPB, Q—the density of nesting MPB, and A—the concentration of beetle pheromone. The model we have chosen allows us to investigate the dynamics of MPB attack in a single summer season where the emergence rate, $\gamma(x, t)$, is determined by the position and severity of MPB attacks in the previous year. That is, given the pattern of MPB attacks in the previous year, we can predict the emergence rate of flying MPB and the resulting pattern of attacks in the current year.

The movement of MPB is described by two processes: diffusion and chemotaxis. These are the first two terms in (1a). The diffusion component describes the random movement of flying MPB, while the chemotaxis describes the attraction and repulsion of MPB according to the concentration of MPB pheromones. MPB have a biological mechanism whereby the pheromone suite is attractive at low densities and repulsive after the concentration becomes too high (White and Powell 1997). As a result, the density of beetles attacking a given tree stays below overcrowding levels (though in epidemic situations, when tree resources are limiting, beetles will attack in higher, suboptimal densities) (Raffa and Berryman 1983).

Our model is structurally similar to the model in Powell et al. (1998), but differs in that the detailed interaction between MPB and lodgepole pine trees in the original model (holes and resin dynamics) has been replaced by a type 3 functional response, $P^2/(P^2 + k_p{}^2)$, multiplied by a random landing rate, $\lambda(x)$. We discuss both of these terms in some detail here, as they frame a novel description of the MPB response to the pheromone and susceptible tree landscape. The random landing rate, $\lambda(x)$, is spatially dependent based on the density of susceptible trees on the landscape. A lower susceptible tree density results in a lower landing rate λ. In this manner, we can include the effects of spatial heterogeneity on the MPB aggregation behaviour. We expect this heterogeneity to affect the spatial distribution of MPB attacks. The type 3 functional response term assumes that the MPB must attack in sufficient densities to successfully nest in a lodgepole pine tree (Safranyik and Wilson 2006). This function is defined such that a low density of attacking beetles has a very low success rate until the MPB density reaches a population threshold, at which point the success of the MPB increases dramatically. This population density threshold is k_p, the MPB density required for 50 % attack success rate. This parameter was estimated based on the empirical data provided in Raffa et al. (1983). For full derivation of k_p see Sect. A.1. All other parameters were based on estimates by Biesinger et al. (2000).

We assume that nesting MPB density, Q, have a small linear death rate, δ_q, since they have successfully penetrated the tree defenses. Once MPB nest they do not move spatially and therefore (1b) contains only reaction terms. In contrast, the suite of MPB pheromones, A, diffuses, is produced by nesting MPB, and has some linear degradation rate, δ_a.

Previous theoretical and empirical work (Biesinger et al. 2000; Raffa and Berryman 1983) informed the selection of parameter values chosen for this study. These values are displayed in Table 1.

2.1 Non-dimensionalization

To simplify model analysis we make the model non-dimensional. The dimensionless variables are:

$$Q = \frac{b_0 \delta_a}{a_1} \overline{Q}, \qquad P = \frac{b_0 \delta_a}{a_1} \overline{P}, \qquad A = b_0 \overline{A},$$

$$t = \frac{1}{\delta_a} \overline{t}, \qquad (x, y) = \sqrt{\frac{\mu_a}{\delta_a}} (\overline{x}, \overline{y}). \tag{2}$$

Table 1 Table of parameter values for the dimensional model (1a)–(1c). Note that the unit 'fh' refers to flight hour of MPB. The parameter k_p was estimated based on emperical data provided in Raffa et al. (1983). All other parameters were based on estimates by Biesinger et al. (2000)

Parameter	Description	Units	Value
μ_p	diffusion of flying MPB	$\frac{ha}{fh}$	1
μ_a	diffusion of beetle pheromones	$\frac{ha}{fh}$	0.648
v_a	beetle pheromone attractiveness	$\frac{ha^2}{\mu g \cdot fh}$	5.7
b_0	concentration of pheromones at which dissipation occurs	$\frac{\mu g}{ha}$	5.4
b_1	concentration at which pheromone is saturated	n/a	1
λ	random landing rate of flying MPB	$\frac{ha}{trees \cdot fh}$	0.16
a_1	rate of pheromone increase due to nesting MPB	$\frac{\mu g}{fh \cdot mpb}$	0.02
k_p	flying beetle density required for 50 per cent success of mass attack	$\frac{mpb}{ha}$	250000
δ_p	death rate of flying MPB	fh^{-1}	0.014
δ_q	death rate of nesting MPB	fh^{-1}	0.001
δ_a	degradation of beetle pheromone	fh^{-1}	180

The choice of non-dimensional scalings can be interpreted biologically. The density of nesting MPB, Q, and the concentration of MPB pheromones, A, were scaled by the density of nesting MPB, 48600 MPB/ha, and the concentration of pheromone (b_0) required for the pheromone to switch from attractive to repulsive, respectively. The density of flying MPB, P, was scaled by the same factor as Q to remain consistent. Time was scaled by the average degradation time of the chemical pheromone. Space was scaled by the average distance that the pheromone will spread before degradation.

Inspection of the parameters in Table 1 reveals order of magnitude differences in the parameter values. We therefore defined a scaling parameter that identifies parameters as relatively small or large when compared to other parameter values. We chose the scaling parameter describing the relative persistence of a pheromone plume, $\frac{1}{\delta_a}$, and the life expectancy of the dispersing MPB, $\frac{1}{\delta_p}$:

$$\epsilon = \frac{\delta_p}{\delta_a}.$$

Since δ_p (death rate of flying MPB) is very small compared to δ_a (degradation rate of MPB pheromone), this ratio is a very small quantity. This order parameter allows us to identify parameters that work over fast and slow scales, respectively. With this scaling parameter we define the following new dimensionless parameters:

$$\overline{\mu_p} = \frac{\mu_p}{\mu_a}, \quad \overline{v_a} = \frac{v_a b_0}{\mu_a}, \quad \overline{k_p} = \frac{k_p a_1}{b_0 \delta_a},$$

$$\overline{\gamma} = \frac{\gamma a_1}{b_0 \delta_a^2}, \quad \epsilon \overline{\delta_q} = \frac{\delta_q}{\delta_a}, \quad \epsilon \overline{\lambda} = \frac{\lambda}{\delta_a}. \tag{3}$$

Table 2 Table of parameter values for the non-dimensional model (4a)–(4c)

Parameter	Value
$\overline{\mu_p}$	1.54
$\overline{\nu_a}$	47.5
ϵ	0.0000778
$\overline{k_p}$	5.14
$\overline{\delta_q}$	0.0714
$\overline{\lambda}$	11.4

Values of the non-dimensional parameters (3) are shown in Table 2. Substituting the non-dimensional parameters (3) and variables (2) into (1a)–(1c), we arrive at

$$\frac{\partial \overline{P}}{\partial \overline{t}} = \overline{\mu_p} \nabla^2 \overline{P} - \overline{\nu_a} \nabla \left(\frac{1 - \overline{A}}{1 + \overline{A}/b_1} \overline{P} \nabla \overline{A} \right) - \epsilon P - \epsilon \overline{\lambda} \frac{\overline{P}^3}{\overline{P}^2 + \overline{k_p}^2} + \overline{\gamma}, \qquad (4a)$$

$$\frac{\partial \overline{A}}{\partial \overline{t}} = \nabla^2 \overline{A} + \overline{Q} - \overline{A}, \qquad (4b)$$

$$\frac{\partial \overline{Q}}{\partial \overline{t}} = -\epsilon \overline{\delta_q Q} + \epsilon \overline{\lambda} \frac{\overline{P}^3}{\overline{P}^2 + \overline{k_p}^2}. \qquad (4c)$$

For the remainder of the paper we will drop the bars above the non-dimensional quantities and assume that we are using the non-dimensional variables and parameter values to simplify notation. The model becomes

$$\frac{\partial P}{\partial t} = \mu_p \nabla^2 P - \nu_a \nabla \left(\frac{1 - A}{1 + A/b_1} P \nabla A \right) - \epsilon P - \epsilon \lambda \frac{P^3}{P^2 + k_p^2} + \gamma, \qquad (5a)$$

$$\frac{\partial A}{\partial t} = \nabla^2 A + Q - A, \qquad (5b)$$

$$\frac{\partial Q}{\partial t} = -\epsilon \delta_q Q + \epsilon \lambda \frac{P^3}{P^2 + k_p^2}. \qquad (5c)$$

3 Model Pattern Formation

The type of pattern formation we investigate is diffusion and chemotaxis-driven instability of a spatially uniform steady state (Murray 2003). Biologically, this amounts to assuming that early in the season emerging MPB are uniformly dispersed on a landscape devoid of chemical information and that hot spots of infestation will develop at spatial scales on which the natural processes of dispersal, attack and pheromone production/dissipation resonate. Often the distribution of previously attacked trees is clustered and non-uniform. Early in the season, however, when beetles are just beginning to emerge, there is no pre-existing chemical information. Consequently, the random dispersal of emerging MPB, coupled with a brief maturation period during

which beetles are not in search of nesting sites (Hughes et al. 2006), together generate a largely uniform distribution of beetles. The distribution is clearly not completely uniform, and the spacing of previously attacked trees should have some effect on the spatial pattern of attack in the following year. This pre-pattern, however, would most likely amplify and accelerate the pattern of MPB attack clusters through a forcing of the inherent spatial resonance. In other words, it is less surprising to see a spatial pattern emerge when it is seeded with a pre-pattern than when it is seeded with no pattern at all. We therefore take the more parsimonious assumption, and set attack and emergence rates to be spatially uniform $\lambda(x) = \lambda$ and $\gamma(x, t) = \gamma(t)$. We additionally set our emergence rate to be constant over time, $\gamma(t) = \gamma$. To investigate potential pattern formation, we find the spatially uniform steady state in Sect. 3.1, then linearize about this steady state and add spatial perturbations to find the dispersion relation in Sect. 3.2 (Murray 2003). This dispersion relation relates the temporal growth of perturbations to the wavenumber of the pattern. This dispersion relation is studied analytically and numerically in Sects. 3.3 and 3.4, to determine the dominant wavenumber of the pattern. This dominant wavenumber predicts the expected spacing between MPB attacks in a given year.

3.1 Spatially Uniform Steady State

To find spatially uniform steady states for (5a)–(5c), all spatial and temporal derivatives are set to zero. The spatially uniform steady state of the model (5a)–(5c) is the solution to the system

$$0 = -\epsilon P - \epsilon\lambda\frac{P^3}{P^2 + k_p{}^2} + \gamma, \tag{6a}$$

$$0 = Q - A, \tag{6b}$$

$$0 = -\epsilon\delta_q Q + \epsilon\lambda\frac{P^3}{P^2 + k_p{}^2}. \tag{6c}$$

Solving (6b) and (6c), we find that there is a spatially uniform steady state given by

$$\left(P^*, A^*, Q^*\right) = \left(P^*, \frac{1}{\delta_q}\lambda\frac{(P^*)^3}{(P^*)^2 + k_p^2}, \frac{1}{\delta_q}\lambda\frac{(P^*)^3}{(P^*)^2 + k_p^2}\right), \tag{7}$$

where P^* is unknown. Rearranging (6a), we obtain a cubic equation

$$P^3 - \frac{\gamma}{\epsilon(1+\lambda)}P^2 + \frac{k_p^2}{1+\lambda}P - \frac{\lambda k_p^2}{\epsilon(1+\lambda)} = 0. \tag{8}$$

The real positive root(s) of this cubic equation (8) will give us the steady state density of flying MPB, P^*. The first derivative of (6a) is always negative and therefore there is only one possible real root. This steady state is positive by inspection of (6a). Emergence rate, γ, is determined exogenously by the density of MPB attack in the

previous year and the temperature (phenology) (Bentz et al. 1996), which will then determine the unique density of dispersing MPB.

This system exhibits three distinct behaviours as the emergence rate, γ, is varied. For very low γ, the flying MPB density, P^*, is very low. At these population levels we have essentially the trivial steady state and the MPB do not successfully attack any trees in the susceptible landscape. If γ is $O(1)$, the largest root scales like $P^* \propto \frac{1}{\epsilon}$. Using this scale one finds that the steady state is approximately

$$(P^*, A^*, Q^*) = \left(\frac{\gamma}{\epsilon(1+\lambda)}, \frac{\lambda}{\delta_q} P^*, \frac{\lambda}{\delta_q} P^* \right). \tag{9}$$

At these emergence rates, P^* is at epidemic densities, and therefore the MPB is successful at inducing mortality in any healthy tree. In contrast, when γ is small, $O(\epsilon)$, the roots of P^* are $O(1)$. When γ is at these values, the population of MPB is not large enough to kill susceptible trees easily, and must successfully aggregate to overcome tree defenses. We will show through our analysis that for a specific intermediate range of γ values, our unique real steady state is an unstable critical point in the presence of diffusion and chemotaxis. Thus, when spatial factors are included, perturbations of the uniform steady state lead to the formation of a spatial pattern. This scale of aggregation will determine the spacing between MPB attacks on a susceptible landscape.

3.2 Linear Analysis

Linearizing about the spatially uniform steady state, we define $f = v_a (\frac{1-Q^*}{1+Q^*/b_1}) P^*$ and $g = \epsilon\lambda \frac{(P^*)^4 + 3(P^*)^2 k_p^2}{((P^*)^2 + k_p^2)^2}$. Note that since $Q^* = A^*$, we replace A^* by Q^* in our equations. We add small spatial perturbations by substituting $P = P^* + \delta P_1$, $Q = Q^* + \delta Q_1$, and ($\delta \ll 1$) $A = A^* + \delta A_1$ into (5a)–(5c) to obtain the perturbation equations,

$$\frac{\partial P_1}{\partial t} = \mu_p \nabla^2 P_1 - f \nabla^2 A_1 - \epsilon P_1 - g P_1, \tag{10a}$$

$$\frac{\partial Q_1}{\partial t} = -\epsilon \delta_q Q_1 + g P_1, \tag{10b}$$

$$\frac{\partial A_1}{\partial t} = \nabla^2 A_1 + Q_1 - A_1. \tag{10c}$$

3.2.1 Method of Annihilators to Find Dispersion Relation

Beginning with (10a)–(10a), we can rewrite these equations in terms of linear differential operators (Nagle et al. 2005):

$$L_1[P_1] = -f L_2[A_1], \tag{11a}$$

$$L_3[Q_1] = g[P_1], \tag{11b}$$

$$L_4[A_1] = [Q_1], \tag{11c}$$

where $L_1 = (\partial_t - \mu_p \partial_{xx} + (\epsilon + g))$, $L_2 = \partial_{xx}$, $L_3 = (\partial_t + \epsilon \delta_q)$, and $L_4 = (\partial_t - \partial_{xx} + 1)$.

From (11a)–(11c) we deduce that $L_1 L_3 L_4 [A_1] = -gf L_2 [A_1]$. If the linear operators are then expanded, we have the equation

$$\big(\partial_t - \mu_p \partial_{xx} + (\epsilon + g)\big)(\partial_t + \epsilon \delta_q)(\partial_t - \partial_{xx} + 1)[A_1] = -gf \partial_{xx}[A_1]. \qquad (12)$$

We assume that the perturbations have an exponential solution of the form $A_1 = c_1 e^{\sigma t + i v_m x}$. This substitution in (12) produces the dispersion relation which links the temporal growth rate, σ, of patterns to their spatial wavenumber, v_m:

$$\big(\sigma + \mu_p v_m^2 + (\epsilon + g)\big)(\sigma + \epsilon \delta_q)(\sigma + v_m^2 + 1) = gf v_m^2. \qquad (13)$$

If the polynomial (13) is expanded in terms of powers of σ, we have

$$\sigma^3 + \sigma^2\big(\epsilon + \mu_p v_m^2 + v_m^2 + g + 1 + \epsilon \delta_q\big) + \sigma\big(\epsilon v_m^2 + \epsilon \delta_q + \mu_p v_m^4$$
$$+ \mu_p v_m^2 \epsilon \delta_q + \mu_p v_m^2 + g v_m^2 + g + g \epsilon \delta_q + v_m^2 \epsilon \delta_q + \epsilon^2 \delta_q + \epsilon\big)$$
$$- gf v_m^2 + g \epsilon \delta_q + \mu_p v_m^4 \epsilon \delta_q + \epsilon^2 v_m^2 \delta_q + g v_m^2 \epsilon \delta_q + \epsilon^2 \delta_q + \mu_p v_m^2 \epsilon \delta_q = 0. \qquad (14)$$

3.3 Analysis of the Dispersion Relation

Before turning to numerical analysis, we first utilize some analytical techniques to find the boundary of the region of maximum pattern formation, and to determine the dominant wavenumber. The dominant wavenumber is the spatial wavenumber that maximizes the temporal growth rate. We rewrite the dispersion relation (14) as

$$p_1 = \sigma^3 + a_2 \sigma^2 + a_1 \sigma + a_0, \qquad (15)$$

where

$$a_2 = \epsilon + \mu_p v_m^2 + v_m^2 + g + 1 + \epsilon \delta_q,$$
$$a_1 = \epsilon v_m^2 + \epsilon \delta_q + \mu_p v_m^4 + \mu_p v_m^2 \epsilon \delta_q + \mu_p v_m^2 + g v_m^2 + g + g \epsilon \delta_q$$
$$\quad + v_m^2 \epsilon \delta_q + \epsilon^2 \delta_q + \epsilon,$$
$$a_0 = -gf v_m^2 + g \epsilon \delta_q + \mu_p v_m^4 \epsilon \delta_q + \epsilon^2 v_m^2 \delta_q + g v_m^2 \epsilon \delta_q + \epsilon^2 \delta_q + \mu_p v_m^2 \epsilon \delta_q.$$

We are interested in situations where pattern formation occurs, that is, where $\sigma_1 = \max_{\alpha \in \mathbb{C}}(\Re(\alpha)|p_1(\alpha) = 0) > 0$. Using Descartes' rule of signs (Smith and Latham 1954), we are able to determine regions in which positive real roots should occur. Descartes' rule of signs counts the number of sign changes of the coefficients of a polynomial to determine the maximum number of real positive roots. Furthermore, if there is a maximum of n real positive roots, the number of allowable roots is $n, n - 2, n - 4, \ldots$ because complex roots must occur in pairs. Therefore, in order for a real positive root to occur, we must have $a_0 < 0$ (one sign change). This is equivalent to the condition

$$gf v_m^2 > g \epsilon \delta_q + \mu_p v_m^4 \epsilon \delta_q + \epsilon^2 v_m^2 \delta_q + g v_m^2 \epsilon \delta_q + \epsilon^2 \delta_q + \mu_p v_m^2 \epsilon \delta_q. \qquad (16)$$

Technically, Descartes' rule of signs limits us to a single positive real root, and either zero or two negative real roots. In the case where there are two negative real roots, we do not need to know anything about these negative real roots, as pattern formation occurs if a single root has a positive real part. When there are not two negative real roots, but $a_0 < 0$, we will argue that the two complex roots have a negative real part.

Assume our cubic has a positive real root r_1 ($r_1 > 0$) and a pair of complex roots $r_2 \pm r_3 i$. The expanded form of the polynomial is:

$$\sigma^3 + \sigma^2(-r_1 - 2r_2) + \sigma\left(2r_1r_2 + r_2^2 + r_3^2\right) - r_1\left(r_2^2 + r_3^2\right). \tag{17}$$

Since $a_2 > 0$ in (15), we must have that $-r_1 - 2r_2 > 0$ in (17). Thus, since $r_1 > 0$ by assumption, we have that $r_2 < 0$. Therefore, in the case where we have a single positive real root and two complex roots, our complex roots must have negative real parts.

In the case where $a_0 > 0$, Descartes' rule of signs determines that there are no positive real roots and that the maximum number of negative real roots are 3. Therefore, there is either 1 or 3 negative real roots to (15). Obviously, in the case of three negative real roots, no pattern formation can occur. There is the possibility of a single negative root, and a pair of complex roots with positive real parts. This case does not occur in the parameter space we explored in the numerical determination of the roots of (15) (see Sect. 3.4).

This means that our pattern formation analysis is restricted to the case where (15) has a single positive real root. We focus on this region when trying to determine the maximum region of pattern formation. Patterns will first form at wavelengths ν_m and parameters chosen such that σ_1 first becomes positive. Therefore, we examine the behaviour of maxima of (15). We know that the maximum pattern formation region with respect to the wavenumber ν_m will occur when $p_2 = \frac{\partial p_1}{\partial(\nu_m^2)} = 0$. The wavenumber at which pattern formation is maximum is called the dominant wavenumber. At this dominant wavenumber, $\frac{\partial \sigma}{\partial(\nu_m^2)} = 0$, thus we can reduce our polynomial (15) to order 2 by taking the derivative. In summary, the dominant wavenumber occurs when $\sigma_1 > 0$, $\sigma_2 = \max_{\alpha \in \mathbb{C}}(\Re(\alpha) | p_2(\alpha) = 0) > 0$, and $\sigma_1 = \sigma_2$. The last condition must be satisfied since both $p_1 = 0$ and $p_2 = 0$ at the dominant wavenumber. Thus we have

$$
\begin{aligned}
p_2 &= \frac{\partial a_2}{\partial \nu_m^2}\sigma^2 + \frac{\partial a_1}{\partial \nu_m^2}\sigma + \frac{\partial a_0}{\partial \nu_m^2}, \\
&= (\mu_p + 1)\sigma^2 + \left(\epsilon + 2\mu_p\nu_m^2 + \mu_p\epsilon\delta_q + \mu_p + g + \epsilon\delta_q\right)\sigma \\
&\quad + \left(-gf + 2\mu_p\nu_m^2\epsilon\delta_q + \epsilon^2\delta_q + g\epsilon\delta_q + \mu_p\epsilon\delta_q\right), \\
&= d_2\sigma^2 + d_1\sigma + d_0.
\end{aligned}
$$

Since $g > 0$, we have that $d_2 > 0$ and $d_1 > 0$. This means that there is exactly one positive real root of p_2 if $d_0 < 0$. Therefore, $\sigma_1 > 0$ if and only if $a_0 < 0$, and $\sigma_2 > 0$ if and only if $d_0 < 0$. Using these conditions we can sketch the region of pattern formation (Fig. 1). Additionally, we numerically calculate (using the method in Sect. 3.4) σ_1 and σ_2 and find the squared difference. If the squared difference is zero,

this signifies a point of intersection between the two curves and a maximum value of σ with respect to v_m^2. In short, the dominant wavenumber occurs at the intersection of σ_1 and σ_2, which is shown on the contour plot.

3.4 Numerical Analysis of the Dispersion Relation

Using a root-finding algorithm in Matlab, we calculated σ_1 while varying γ, the emergence rate (of flying MPB) at steady state, and v_m, the spatial wavenumber. The contour plot produced is shown in Fig. 1. Additionally, we show the two-dimensional plot of growth rate with respect to wavenumber. This curve shows the maximum growth rate with respect to emergence rate at each wavenumber. In our calculations we scaled the wavenumber, v_m, so that it would be the reciprocal of wavelength. The wavelength w_m can be calculated as

$$w_m = \frac{2\pi}{v_m}. \tag{18}$$

The maximal eigenvalue of $8.04\mathrm{e}^{-5}$ in the contour plot is dimensionless, and when redimensionalized becomes $0.0145\ \mathrm{fh}^{-1}$, which is an appropriate timescale for pattern formation within a single summer (corresponding to 80 fh, or 2–4 weeks of the flight season). The maximal eigenvalue occurred at the dominant wavenumber of 2.74 km^{-1}, with an emergence rate of 300 MPB/(ha fh). Assuming an output of approximately 10,000 MPB/tree per flight season (Powell and Bentz 2009), this corresponds to approximately 2–3 source trees/ha. The resulting steady state density of nesting MPB is $Q^* \approx 20100$ MPB/ha. Using the conversion of 800 nesting MPB/tree (Powell and Bentz 2009), we find the resulting number of killed trees due to this attack is approximately 25. Therefore, this pattern of aggregation is important for the transition in-between incipient epidemic and epidemic densities of MPB. In an incipient epidemic (Safranyik and Wilson 2006), the MPB population can form small clusters of attack rather than attacks occurring on large tracts of continuous forest. These source densities would describe the transition from incipient epidemic to epidemic densities.

There is a strong agreement between the analytical and numerical determinations of the dominant wavenumber and the region of pattern formation. The analytical method correctly identifies the region where there is a single positive root, and from Fig. 1 this is exactly the same as the region where $\sigma_1 > 0$ (pattern formation occurs). Additionally, the wavenumber at which $\sigma_1 = \sigma_2$ in Fig. 1 verifies the numerical calculation of the dominant wavenumber at 2.74 km^{-1}, which corresponds to a wavelength of 364 m. Thus, our analytical and numerical works yield the prediction that attack clusters during the transition between incipient epidemic and epidemic population levels will be approximately 364 m apart. This prediction is based on our model assumptions which include landscape homogeneity, chemotactic response of MPB due to pheromone (both attractive/repulsive), and a type-3 functional response describing the transition between flying and nesting MPB.
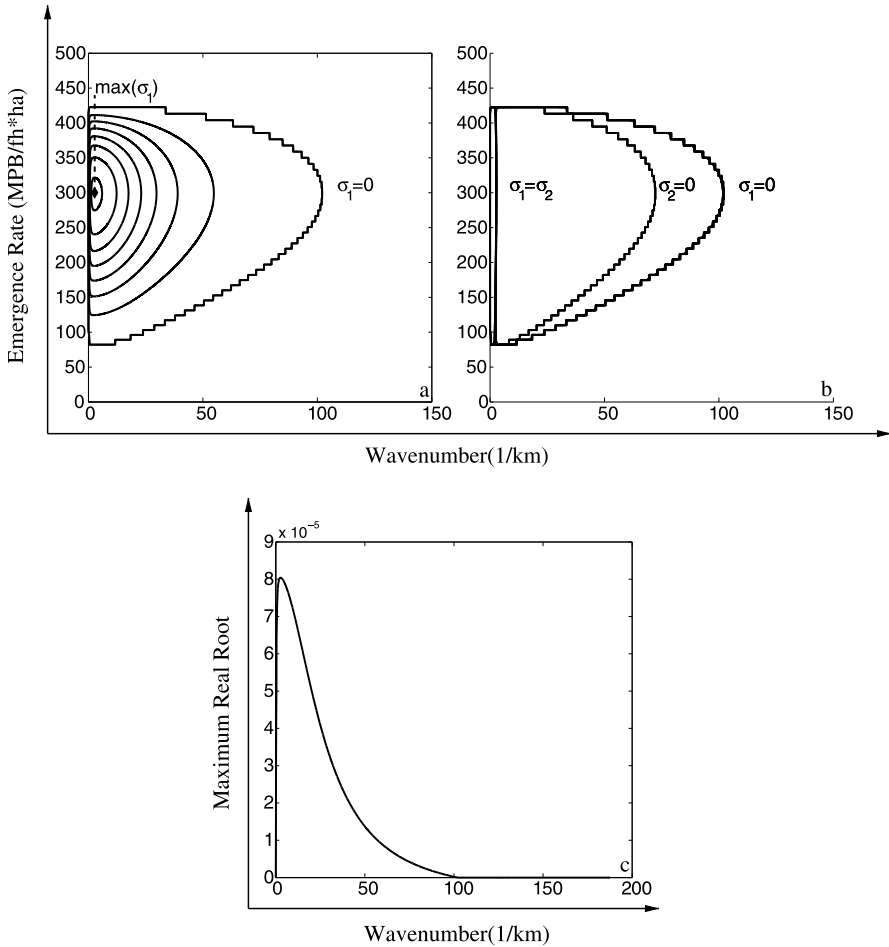
Fig. 1 Numerical contour plot of the temporal growth rate, σ_1, against wavenumber and emergence rate of MPB (**a**). The maximum value of σ_1 is labeled with a diamond at (2.74, 299). The surface is unimodal with a single maximum. The analytical contour plot of temporal growth rate against wavenumber and emergence rate of MPB is shown in (**b**). The contour plot in (**b**), uses the analysis of the dispersion relation to find the region of pattern formation ($\sigma_1 = 0$), and the dominant wavenumber ($\sigma_1 = \sigma_2$). The contour plot in (**a**), shows the region of pattern formation and the dominant wavenumber as determined numerically. The final plot (**c**), is a horizontal slice of the surface in (**a**) at a fixed emergence rate, $\gamma = 299$ MPB/(fh ha). This curve demonstrates how well defined the peak is in the $\sigma_1(\nu_m, \gamma)$ surface

4 Data Analysis

The second component of this project was to compare spatial data of MPB attacks to the model predictions. We analysed MPB attack data from the Sawtooth National Recreation Area (SNRA), located in the Rocky Mountains of central Idaho, to identify any characteristic distances between patches of beetle infestation. Data was provided by USDA Forest Service aerial detection survey (ADS) in and around the SNRA. Full details are provided in Crabb et al. (2012). The data set extends over

a period of 19 years, 1991–2009. The data are remarkably detailed, taken at a grid-scale of 30 m over a region of 275,776 ha. All 19 years include regions where MPB are at incipient epidemic densities; many of these years also have regions with epidemic densities of MPB. Thus, this data tracks the progression of an MPB epidemic as captured by dead (red top) trees. Trees develop a red top the following summer after being attacked as a result of beetle-induced mortality. The initial attacks at incipient epidemic levels resulted in small clusters of dead trees. During the 19 years, many of these populations had risen to epidemic levels and killed a more significant portion of the available pine trees over the landscape. The later years of this data set capture the period after the epidemic where the MPB population density has decreased to lower levels. For the purposes of our analysis the data was defined with ones given to grid cells (locations) of MPB attack, and zeroes given to locations with no MPB attack.

The data sets chosen for analysis in each year were from areas of incipient epidemic MPB population densities, consistent with the assumptions used in the linearization of the model. That is, we selected regions with small spots ($\leq$300 m in diameter) of MPB attack and at least 5 spots per region. For the size of these regions, we picked the largest region such that these two conditions were satisfied. The error in the computation of wavenumber decreased as the size of the chosen region increased because larger regions increased resolution in Fourier space. To calculate the distance between spots of MPB attack we used discrete fast Fourier transform. Discrete Fourier transform assumes that the data can be decomposed into a finite number of sine and cosine functions on a grid. The process returns the amplitude of these sine and cosine functions, the wavenumbers with the largest amplitude best describe the scale of aggregation of MPB attack in the data. The particular DFT used was Matlab's fft2, with which we calculated the radial wavenumber, ν_r:

$$\nu_r = \sqrt{\nu_x^2 + \nu_y^2}, \tag{19}$$

where ν_x and ν_y are spatial wavenumbers of the data in the x and y directions. Since DFT returns the amplitude of both the sine and cosine components of the data, we need to compute the power, which is the squared complex modulus of the amplitude. This factors both the sine and cosine amplitudes at each wavenumber into a single value, the power. An example region and power spectral density is shown in Sect. A.2 (Fig. 4).

We are interested mainly in the wavenumber at which the power is maximum. This is called the dominant wavenumber and is the most influential wavenumber represented in the data. To have error bounds we computed the upper (ν_u) and lower (ν_l) bounds for the dominant wavenumber, ν_d, which were chosen such that:

$$\nu_l = \left\{ \min(\nu) | m(\nu) \geq 0.80 m(\nu_d) \right\},$$
$$\nu_u = \left\{ \max(\nu) | m(\nu) \geq 0.80 m(\nu_d) \right\},$$

where $m(\nu)$ is the power at the wavenumber, ν.

Fig. 2 Average dominant wavenumber over years 1991–2009. ν_d refers to the average dominant wavenumber, ν_l and ν_u refer to the lower and upper bounds on ν_d, Mean(ν_d) refers to the average of the dominant wavenumber over all years, and $\nu_{d,\text{model}}$ refers to the model predicted dominant wavenumber. This graph shows the trend in ν_d over the years 1991–2009. Points where ν_u and ν_l are near ν_d represent years in the data where the power spectral density shows a very large sharp peak at the given ν_d
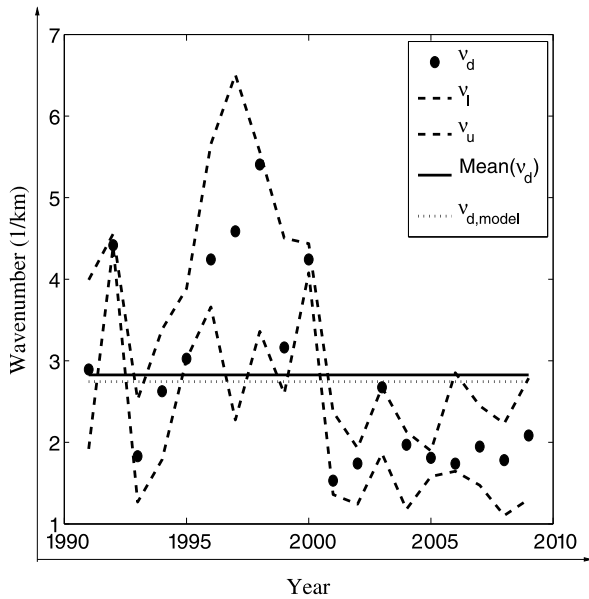
Since multiple regions were chosen in each year, the average dominant wavenumber in a given year was calculated as a weighted average based on the power:

$$\nu_d = \Sigma_i \left(\frac{m_i}{\Sigma_j m_j} \nu_i \right), \tag{20}$$

where ν_i is the dominant wavenumber for region i and m_i is the power at the maximum. Average upper and lower bounds for each year were calculated similarly.

The average dominant wavenumber in each year is displayed in Fig. 2 over 1991–2009. The average dominant wavenumber varies between 1.5 and 5.5 km^{-1}. The dominant wavenumber appears to be higher in 1991–2000 than in the years 2001–2009. The mean dominant wavenumber is calculated to be 2.83 km^{-1}, which is very close to the model predicted dominant wavenumber of 2.74 km^{-1}.

The frequency of each dominant wavenumber independently of year is given in Fig. 3. The dominant wavenumber from the model, $\nu_{d,\text{model}}$, is validated by the data, as it is close to the centre of the distribution of ν_d. In fact, the majority of ν_d appearing is enclosed between the lower ($\nu_{l,\text{model}}$) and upper ($\nu_{u,\text{model}}$) bounds on the model dominant wavenumber.

A weighted histogram was also produced, where each count is scaled by the relative power at that ν_d. This measure is important as it highlights the wavenumbers which more strongly represent patterns in MPB attacks in the data. Similarly to the first histogram, $\nu_{d,\text{model}}$ provided a good estimate of the centre of the distribution of ν_d (data), and a large proportion the distribution of ν_d was effectively captured within the range between $\nu_{l,\text{model}}$ and $\nu_{u,\text{model}}$.

Fig. 3 The histogram of dominant wavenumbers over all years (**a**) and the histogram weighted by the power at each dominant wavenumber over all years (**b**). The *solid line* is the model dominant wavenumber and the *dotted lines* are upper (5.5069 km^{-1}) and lower (1.3783 km^{-1}) bounds on the model dominant wavenumber
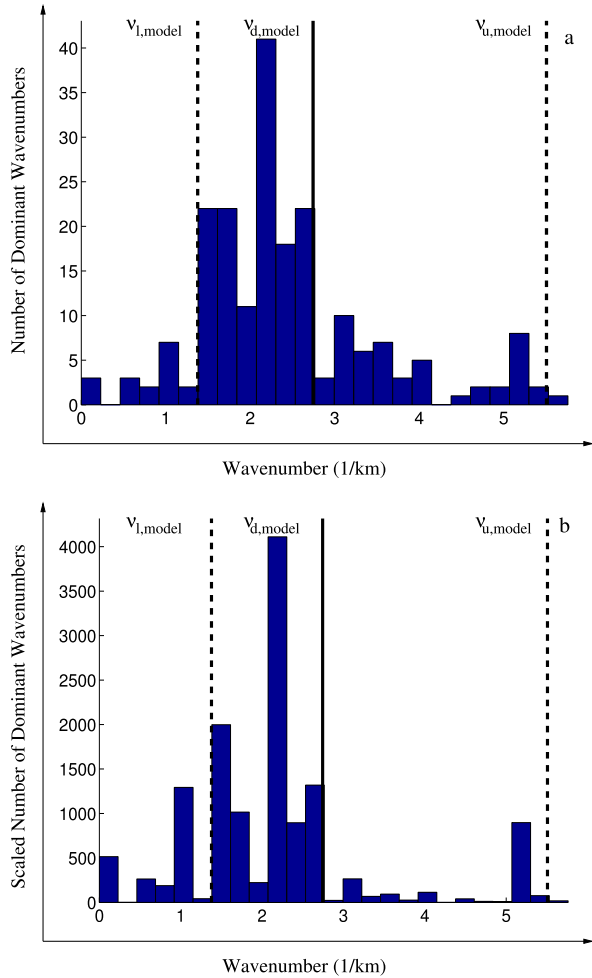
For the histogram, the upper and lower bounds for the model dominant wavenumber were chosen such that:

$$\nu_{l,\text{model}} = \left\{ \min(\nu) | \sigma_1(\nu) \geq 0.975\sigma_1(\nu_{d,\text{model}}) \right\},$$

$$\nu_{u,\text{model}} = \left\{ \max(\nu) | \sigma_1(\nu) \geq 0.975\sigma_1(\nu_{d,\text{model}}) \right\},$$

where $\sigma_1(\nu)$ is the growth rate at the wavenumber, ν.

We found an interesting trend when analysing the data: as time progressed, the spots of MPB attack became larger and farther apart (results not shown). This trend in the spot pattern is intriguing and it would be valuable to investigate if this trend is characteristic of the progression of an MPB epidemic.

5 Discussion

Model pattern formation analysis predicts a dominant wavenumber of 2.74, or spots of MPB attack that are 364 m apart. Analysis of SNRA spot data indicates spots are 353 m apart on average, with a wavenumber of 2.83, only a 3 % difference between the model predictions and field observations. Since our model was parameterized completely independently of the SNRA data, this correspondence between the model and data gives a strong validation of our model.

Our analysis indicates that it might be possible to use pheromone baits to disrupt the aggregation process. Our modelling approach could be used to determine whether or not judicious placement of pheromone baits could completely or partially hinder the formation of spot aggregates, and the number and placement of baits necessary to prevent the transition from incipient epidemic to epidemic.

Past forestry practices and fire suppression has given rise to homogeneous and even-age stands of lodgepole pine which has led to large outbreaks of MPB (Samman and Logan 2000). Numerical simulations of the model could be used to determine what types of heterogeneous distributions of susceptible trees (in homogeneous and mixed-forest stands) would interfere with the natural pattern formation of MPB attack clusters. In particular, it might be possible to find tree distributions that would make it impossible (or very difficult) for MPB to transition from endemic to epidemic densities.

Our model assumes the habitat is homogeneous and therefore the wavelength between attacks formed by MPB predicted in our model is driven by the intrinsic biology of the MPB. This means that at incipient epidemic densities there can be development of aggregation pattern that is driven by the MPB movement dynamics and not heterogeneities in the landscape. A previous study by White and Powell (1997) found that the patterns observed at endemic densities were driven by the landscape, while patterns observed at the epidemic densities are driven by the self-focusing dynamics of the MPB. Our study adds to this work by finding that the patterns at the incipient epidemic density (between the endemic and epidemic levels studied by White and Powell) can be explained by the MPB biology.

Our results are fairly robust to changes in parameter values. Parameter sensitivity analysis showed that our model wavelength prediction is most sensitive to increases in $\overline{\mu_p}$, the diffusion rate of MPB. This result is expected, intuitively, as diffusion is known to smooth patterns when pattern formation is driven by chemotaxis. All parameters were altered by 10 % (while keeping all other parameters constant), and the most sensitive parameter, $\overline{\mu_p}$, only changed the wavelength prediction by at most 3.8 %. This means that our pattern formation analysis is relatively insensitive to parameter changes. Parameter sensitivity was measured as a ratio of standardized changes in wavenumber to standardized changes in parameter values (Haefner 2005). Future work needs to investigate the effects of varying multiple parameters simultaneously.

An important factor not included in our model is the effect of temperature, which has been shown to have a significant effect on MPB emergence and spread (Aukema et al. 2008; Gilbert et al. 2004; Powell and Bentz 2009). If temperature changes, through global warming (Logan and Powell 2001; Powell and Logan 2005), habitats

that were previously unsuitable for MPB may become suitable. Additionally, temperature changes can increase the synchrony of emergence, which could increase the density of MPB attacks and allow for spot formation. An interesting extension of our mathematical model would explore how the predicted wavelength changes as this factor is included. This could be done by making the emergence rate, γ, a function of temperature. This modification would add a new layer to the complexity of the pattern formation analysis, and may require numerical simulations to determine the expected wavelength between clusters in a given landscape.

From an analytical standpoint, it would be interesting to complete the second-order perturbation analysis of these equations (Murray 2003; Tyson 1996). We only investigate spot aggregation patterns in the present work, but it may be that other patterns are possible. An understanding of the possible aggregation patterns would provide managers with an additional tool for gauging the MPB population level and risk of an epidemic.

A final interesting extension of our work would be to determine the time it takes for the MPB population to reach epidemic levels once the characteristic wavelength of pattern formation (364 m) has been established. In order to do this, the model would require a between-season component to describe the over-winter reproduction and development of MPB. This study is currently in progress.

Our modelling approach can be applied to other organisms that exhibit patchy spread (Shigesada et al. 1995). Examples include birds such as house finches (Lewis and Pacala 2000), sparrows, and starlings (Shigesada et al. 1995). Additionally, there are insects who exhibit patchy spread, such as are rice weevils (Shigesada et al. 1995), emerald ash borer, leaf-miner moth, pinewood nematode, corn rootworm (Carrasco et al. 2010), and gypsy moth (Petrovskii and McKay 2010). Some plants, such as cheat grass (Lewis and Pacala 2000), also exhibit patchy spread. Note that the patchiness of the MPB spread is an inherent property of the chemotactic behaviour of the insects. The patchy spread exhibited by the other organisms listed here may or may not be due to the same mechanism and comparisons would be both interesting and instructive. Many of the populations mentioned are invasive species and so an understanding of their spatial invasion dynamics is vitally important, as invasive species can devastate populations of native flora and fauna (Mack et al. 2000).

Appendix

A.1 Estimating Allee Attack Threshold, k_p

The parameter k_p is the density of flying MPB required for 50 % nesting beetle success. Assuming each female beetle makes a single gallery, we estimate the density of flying MPB required for a 50 per cent success of mass attack to be 40 beetles/m^2
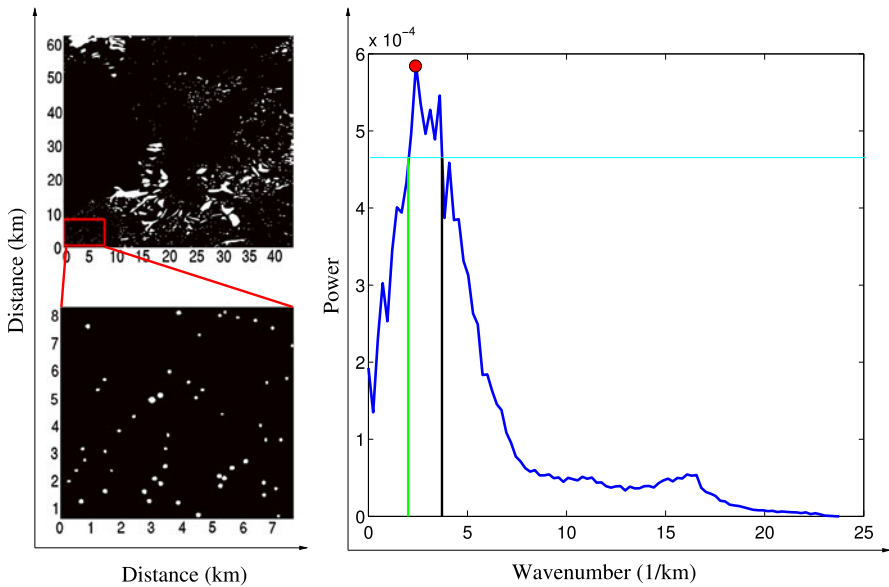
Fig. 4 The SNRA (*top left*) is plotted for 2007, where white areas denote regions of MPB attack. The *red highlighted region* (*left bottom*) is analysed using Discrete fast Fourier transforms to determine the power spectral density (*right*). In this graph, the dominant wavenumber (ν_d) is represented by a solid *red dot*, and the upper (ν_u) and lower (ν_l) bounds on the dominant wavenumber are displayed with *vertical green* and *black lines*, respectively (Color figure online)

(Raffa and Berryman 1983). Since our model uses area in ha instead of m^2, we must multiply this quantity by a conversion factor

$$B_h = B_m \frac{SA}{TA}, \tag{21}$$

where B_h is the number of beetles per hectare, B_m is the number of beetles per m^2, *SA* is the surface area of the tree attacked, and *TA* is the area within which a beetle is considered to be "attacking" a tree.

Assuming that the basal 7.5 m of a tree can be attacked (Raffa and Berryman 1983), we find the surface area as $SA = \pi dh$, where the tree diameter, d, can range from 0.1874 to 0.3456 m and the height h is taken to be 7.5 m. Therefore, *SA* can range from 4.42 to 8.14 m^2. We assume that beetles will attack within a 10 m^2 area of the tree, $TA = 10$ m$^2 = 10^{-3}$ ha, which makes $k_p = 176800$–325600 beetles/ha. We initially assume the value of $k_p = 250000$ MPB/ha.

A.2 FFT Analysis of MPB Data

An example of the FFT analysis of the data (in 2007) is shown in Fig. 4. Each year the landscape was analysed for regions of incipient epidemic densities of MPB. The size and number of regions chosen in each year is displayed in Fig. 5.
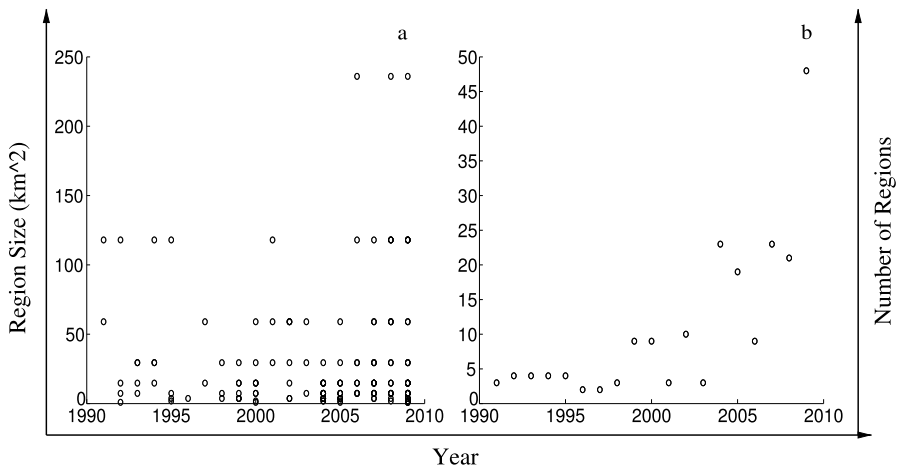
Fig. 5 The size (km^2) (**a**) and number of regions (**b**) over the time period 1991–2009. Multiple regions of the same size in the same year are represented by a *single dot* for clarity

References

Aukema, B. H., Carroll, A. L., Zheng, Y., Zhu, J., Raffa, K. F., Moore, R. D., Stahl, K., & Taylor, S. W. (2008). Movement of outbreak populations of mountain pine beetle: influences of spatiotemporal patterns and climate. *Ecography*, *31*, 348–358.

Bentz, B. J., Powell, J. A., & Logan, J. A. (1996). Localized spatial and temporal attack dynamics of the mountain pine beetle in lodgepole pine. *Intermountain Research Paper*, *494*.

Biesinger, Z., Powell, J., Bentz, B., & Logan, J. (2000). Direct and indirect parameterization of a localized model for the mountain pine beetle-lodgepole pine system. *Ecol. Model.*, *129*, 273–296.

Brooks, J. E., & Stone, J. E. (2003). *Mountain pine beetle symposium: challenges and solutions*. Natural Resources Canada, Canadian Forest Service, Pacific Forestry Centre, Victoria, BC.

Budrene, E. O., & Berg, H. C. (1991). Complex patterns formed by motile cells of Escherichia coli. *Nature*, *349*(6310), 630–633.

Budrene, E. O., & Berg, H. C. (1995). Dynamics of formation of symmetrical patterns by chemotactic bacteria. *Nature*, *376*(6535), 49–53.

Burnell, D. G. (1977). A dispersal-aggregation model for mountain pine beetle in lodgepole pine stands. *Res. Popul. Ecol.*, *19*, 99–106.

Carrasco, L. R., Mumford, J. D., MacLeod, A., Harwood, T., Grabenweger, G., Leach, A. W., Knight, J. D., & Baker, R. H. A. (2010). Unveiling human-assisted dispersal mechanisms in invasive alien insects: integration of spatial stochastic simulation and phenology models. *Ecol. Model.*, *221*, 2068–2075.

Crabb, B. A., Powell, J. A., & Bentz, B. J. (2012). *Development and assessment of 30-m pine density maps for landscape-level modeling of mountain pine beetle dynamics*. USDA FS Rocky Mountain Research Station Research Note.

Gamarra, J. G. P., & He, F. (2008). Spatial scaling of mountain pine beetle infestations. *J. Anim. Ecol.*, *77*, 796–801.

Geiszler, D. R., Gallucci, V. F., & Gara, R. I. (1980). Modeling the dynamics of mountain pine beetle aggregation in a lodgepole pine stand. *Oecologia (Berl.)*, *46*, 244–253.

Gilbert, E., Powell, J. A., Logan, J. A., & Bentz, B. J. (2004). Comparison of three models predicting developmental milestones given environmental and individual variation. *Bull. Math. Biol.*, *66*, 1821–1850.

Haefner, J. W. (Ed.) (2005). *Modeling biological systems*. New York: Springer.

Heavilin, J., & Powell, J. (2008). A novel method of fitting spatio-temporal models to data, with applications to the dynamics of mountain pine beetles. *Nat. Resour. Model.*, *21*(4), 489–524.

Hughes, J., Fall, A., Safranyik, L., & Lertzman, K. (2006). *Modeling the effect of landscape pattern on mountain pine beetles*. Technical report BC-X-407, Natural Resources Canada, Canadian Forest Service, Pacific Forestry Centre, Victoria, British Columbia.

Lewis, M. A., & Pacala, S. (2000). Modeling and analysis of stochastic invasion processes. *J. Math. Biol.*, *41*, 387–429.

Logan, J. A., & Powell, J. A. (2001). Ghost forests, global warming and the mountain pine beetle (coleoptera) Scolytidae. *Am. Entomol.*, *47*, 160–173.

Logan, J. A., White, P., Bentz, B. J., & Powell, J. A. (1998). Model analysis of spatial patterns in mountain pine beetle outbreaks. *Theor. Popul. Biol.*, *53*, 236–255.

Mack, R. N., Simberloff, D., Lonsdale, W. M., Evans, H., Clout, M., & Bazzaz, F. (2000). Biotic invasions: causes, epidemiology, consequences, and global control. *Issues Ecol.*, *5*, 1–20.

Mitchell, R. G., & Preisler, H. K. (1991). Analysis of spatial patterns of lodgepole pine attacked by outbreak populations of the mountain pine beetle. *For. Sci.*, *37*(5), 1390–1408.

Murray, J. D. (2003). *Mathematical biology*. Berlin: Springer.

Nagle, R. K., Saff, E. B., & Snider, A. D. (Eds.) (2005). *Fundamentals of differential equations and boundary value problems*. Boston: Pearson.

Peltonen, M., Liebhold, A. M., Bjornstad, O. N., & Williams, D. W. (2002). Spatial synchrony in forest insect outbreaks: roles of regional stochasticity and dispersal. *Ecology*, *83*(11), 3120–3129.

Pérez, L., & Dragićević, S. (2011). ForestSimMPB: a swarming intelligence and agent-based modeling approach for mountain pine beetle outbreaks. *Ecol. Inform.*, *6*, 62–72.

Petrovskii, S., & McKay, K. (2010). Biological invasion and biological control: a case study of the gypsy moth spread. *Asp. Appl. Biol.*, *104*, 37–48.

Polymenopoulos, A. D., & Long, G. (1990). Estimation and evaluation methods for population growth models with spatial diffusion: dynamics of mountain pine beetle. *Ecol. Model.*, *51*, 97–121.

Powell, J., & Bentz, B. (2009). Connecting phenological predictions with population growth rates for mountain pine beetle, an outbreak insect. *Landsc. Ecol.*, *24*, 657–672.

Powell, J. A., & Logan, J. A. (2005). Insect seasonality – circle map analysis of temperature-driven life cycles. *Theor. Popul. Biol.*, *67*, 161–179.

Powell, J. A., Mcmillen, T., & White, P. (1998). Connecting a chemotactic model for mass attack to a rapid integro-difference emulation strategy. *SIAM J. Appl. Math.*, *59*(2), 547–552.

Raffa, K. F., & Berryman, A. A. (1983). The role of host plant resistance in the colonization behaviour and ecology of bark beetles (coleoptera) scolytidae. *Ecol. Monogr.*, *53*(1), 27–49.

Riel, W. G., Fall, A., Shore, T. L., & Safranyik, L. (2004). *A spatiotemporal simulation of mountain pine beetle impacts on the landscape*. Technical report BC-X-399, Natural Resources Canada, Canadian Forest Service, Pacific Forestry Centre, Victoria, British Columbia.

Robertson, C., Nelson, T. A., Jelinski, D. E., Wulder, M. A., & Boots, B. (2009). Spatial-temporal analysis of species range expansion: the case of the mountain pine beetle, Dendroctonus ponderosae. *J. Biogeogr.*, *36*(8), 1446–1458.

Safranyik, L. & Wilson, B. (Eds.) (2006). *The mountain pine beetle*. Natural Resources Canada, Canadian Forest Service, Pacific Forestry Center, Victoria, BC, Canada.

Safranyik, L., Barclay, H., Thomson, A., & Riel, W. G. (1999). *A population dynamics model for the mountain pine beetle, Dendroctonus ponderosae Hopk.* (coleoptera: Scolytidae). Technical report BC-X-386, Natural Resources Canada, Canadian Forest Service, Pacific Forestry Centre, Victoria, British Columbia.

Samman, S., & Logan, J. (2000). Assessment and response to bark beetle outbreaks in the rock mountain area. Technical report RMRS-GTR-62, U.S. Department of Agriculture, Forest Service, Rocky Mountain Research Station, Ogden, UT, U.S.

Shigesada, N., Kawasaki, K., & Takeda, Y. (1995). Modeling stratified diffusion in biological invasions. *Am. Nat.*, *146*(2), 229–251.

Smith, D. E., & Latham, M. L. (1954). *The geometry of Rene Descartes with a facsimile of the first edition*. New York: Dover.

Turing, A. M. (1952). The chemical basis of morphogenesis. *Philos. Trans. R. Soc. Lond. B*, *237*, 37–72.

Tyson, R. C. (1996). *Pattern formation by E. coli - mathematical and numerical investigation of a biological phenomenon*. PhD thesis, University of Washington.

Tyson, R., Lubkin, S. R., & Murray, J. D. (1999). Model and analysis of chemotactic bacterial patterns in a liquid medium. *J. Math. Biol.*, *38*(4), 359–375.

White, P., & Powell, J. (1997). Phase transition from environmental to dynamic determinism in mountain pine beetle attack. *Bull. Math. Biol.*, *59*, 609–643.